



Recycled aggregate concrete: Localized failure assessment in thermodynamically consistent non-local plasticity framework



Marianela Ripani^{a,*}, Guillermo Etse^{a,b}, Sonia Vrech^b

^a Universidad de Buenos Aires. Consejo Nacional de Investigaciones Científicas y Técnicas (CONICET). Instituto de Tecnologías y Ciencias de la Ingeniería "Hilario Fernández Long" (INTECIN). Facultad de Ingeniería, Buenos Aires, Argentina

^b CONICET, Center for Numerical and Computational Methods in Engineering, National University of Tucumán, Argentina

ARTICLE INFO

Article history:

Received 31 March 2016
Accepted 17 August 2016
Available online 24 October 2016

Keywords:

Gradient plasticity
Thermodynamic consistency
Recycled aggregate concrete

ABSTRACT

A gradient plasticity theory is extended to predict the mechanical failure behavior of concrete with recycled aggregates. A relevant feature of the novel constitutive formulation is its full consistency with the thermodynamic laws regarding hardening and softening response behaviors. The proposed model includes a formulation of a maximum strength surface which is dependent on the recycled aggregate content. While the hardening law is formulated in the framework of classical-local elastoplasticity, the post-peak behavior is described by means of a non-local gradient and fracture-energy-based law. Thereby, the gradient and fracture-energy characteristic lengths are described in terms of the acting confining pressure and the recycled aggregate content. The formulation of the proposed constitutive theory is complemented by the description of the associated localization indicator, based on the acoustic or localization tensor. Finally, numerical results are presented to demonstrate the predictive capabilities of the proposed model and the performance of the localization indicator for different critical stresses and recycled aggregate contents.

© 2016 Elsevier Ltd. All rights reserved.

1. Introduction

Global warming is a major issue of the civilization nowadays and certainly in the next future. Among the different industries, the construction sector is one of the most energy consuming [1]. In this context, the use of recycled aggregates in the fabrication of concrete offers a very interesting approach to reduce energy consume and contamination. Recently, numerous researches have addressed the possible structural use of concrete with the addition of recycled aggregates [2,3]. Moreover, several building codes [4,5] have reflected the knowledge improvements made by the international scientific community on the mechanical behavior of recycled aggregate concretes (RAC). Although RAC is a relatively new material and due to the significant potential it has in the construction industry, numerous research activities were already performed. From the experimental point of view we may refer here to the contributions by Kou and Poon [6], Lima et al. [7], and Folino and Xargay [8]. These studies demonstrated that even though some relevant mechanical properties of RAC, such as compressive and tensile strengths and its elasticity modulus, may be lower than

those of Natural Aggregate Concrete (NAC), the overall mechanical behavior of RAC is still appropriated for structural use.

As it is well known, the failure mechanism of concrete does strongly depend on three main items. One of them, the governing stress or, more precisely, the confinement level is a boundary condition. The others are the aggregate physical features (namely type and size) which control the fracture energy released during brittle failure modes, and the chemical characteristics of its micro and mesostructure, which strongly influence the overall performance of concrete materials. In case of RACs and due to the effect of the recycled aggregates and of the imperfect bonding between them and the surrounding mortar both, the fracture energy and the overall performance are affected when compared to concrete made with natural aggregates. Regarding the modeling of the degradation and post-peak behavior of concrete, different criteria were followed due to the quite diverse failure mechanisms of this material. As it is widely recognized, in the tensile and low confinement zones of concrete maximum strength surface, its mechanical response turns highly brittle and this situation becomes more critical by the presence of recycled aggregates. The failure ductility in the related post-peak regimes can be objectively described by means of the well-known fracture energy released during concrete cracking process. Therefore, fracture energy-based continuum approaches in the framework of the flow theory of plasticity, see

* Corresponding author.

E-mail addresses: mripiani@fi.uba.ar (M. Ripani), getse@herrera.unt.edu.ar (G. Etse), svrech@herrera.unt.edu.ar (S. Vrech).

a.o. Etse and Willam [9], Comi and Perego [10]; or of the continuum damage theory, see a.o. Bazant and Oh [11], Oliver [12], were recurrently considered in the literature to model brittle post-peak behaviors of concrete. Thereby, a characteristic length is introduced which relates the crack opening displacement of the real discontinuum to the involved strain of the equivalent continuum and, in turn, allows objective predictions of the load-displacement response behavior. On the other hand, in medium and high confinement zones of concrete maximum strength surface, its failure mechanism is characterized by multiple and strongly distributed microdefects. Thus, the relevant parameter controlling the mechanical behavior of concrete is the characteristic length defining the microdefect diffusion, which increases with the applied confinement, instead of the fracture energy released in concentrated cracks. This includes the case of RAC. In the realm of the smeared crack approach, the gradient based constitutive theories (see a.o. Vardoulakis and Aifantis [13], Comi [14], and Simone et al. [15]) are the most appropriate ones to objectively describe non-local effects in the framework of diffuse failure processes, leading to fully mesh-independent predictions of the microdefect diffusion zones. Actually, gradient-based constitutive equations provide an effective theoretical framework to resolve the gap between macro and micro-mechanical levels of observation [16–18]. Among the proposals related to the use of gradient based theories in concrete modeling, we refer here to the contributions by Peerlings et al. [19], Pan et al. [20], and Peerlings et al. [21]. These two different approaches (non-local gradient theory and fracture energy-based formulations) for constitutive model formulations of concrete failure processes were, so far, alternatively considered. However, the highly complex variation from brittle to ductile failure modes of concrete requires special provisions for constitutive theories to accurately describe the whole spectrum of possible failure mechanisms. Therefore, a combination of both modeling approaches is required to accurately describe the whole spectrum of concrete failure modes within one single constitutive theory. The first consideration in this regard was due to Vrech and Etse [22] who proposed a fracture energy and gradient-based constitutive model for concrete including two characteristic lengths. One of them accounting for the fracture energy released during brittle and quasi-brittle failure modes in the tensile and low confinement regimes, while the other one is related to the gradient formulation which describes the degradation of the material located in between active cracks during failure processes in the medium and high confinement regimes. In this line, Ripani et al. [23] extended the combined fracture energy and gradient based theory for the case of porous media subjected to non-uniform temperature conditions to model the behavior of concrete failure behavior under high temperature. This theoretical framework is considered in this work to model the particular failure behavior of RAC as this material shows more brittle behavior as classical concrete, while the same ductility capacity in the high confinement regime.

On the other hand, after concrete crushing, a thin layer of cement paste remains adhered to the original aggregate surface and, for that reason, the recycled concrete aggregates have a greater porosity than natural ones. This changes the morphology of the interface transition zones and strongly affects the failure behavior of RAC (see, Poon et al. [24], Corinaldesi [25], Casuccio et al. [26], Xiao et al. [27]). Consequently, the percentage of replacement of natural coarse aggregates by recycled ones strongly reduces the uniaxial compression strength and it is a fundamental parameter to be considered in the prediction of the mechanical properties of RAC [8]. So far, very few constitutive formulations have been proposed to predict the mechanical behavior of RAC. They are mainly oriented to predict the uniaxial compression stress-strain behavior [28,29]. In fact, none of the existing proposals are able to accurately reproduce the entire spectrum of possible

failure modes of RAC when subjected to different loading paths and for arbitrary proportions of recycled aggregates.

In this paper, a reformulation of the so-called Leon-Drucker-Prager (LDP) model for NAC [22] is proposed to predict the mechanical response of RAC, where the variation from ductile to brittle failure is accomplished by means of the pressure dependent formulation of both characteristic lengths: the fracture energy-based length and the gradient-based one. The effects of the recycled aggregates on the overall mechanical response behavior of RAC is taken into account by means of the so-called *concrete mixture recycling factor* which mainly depends on the percentage of replacement of natural aggregates by recycled ones, which as mentioned above, is directly related to the strength loss of the recycled aggregate concrete. This factor is introduced in the proposed reformulation of the hardening and softening laws and it is also taken into account in defining the degradation of the maximum strength criterion and of the non-associated plastic potential. One of the main advantages of this model focuses on the definition of this single parameter, the concrete mixture recycling factor, which must be experimentally calibrated to represent the influence of the recycled aggregates on the mechanical behavior of RAC. These aggregates could derive from different origins and their different effects on RAC are evaluated by means of the calibration of the concrete mixture recycling factor. Consequently, this factor constitutes a macroscopic degradation parameter which quantifies the degradation of the concrete mechanical properties depending on the quantity and quality of recycled aggregates. In this work, the concrete mixture recycling factor is calibrated for the particular case of aggregates obtained from the demolition of concrete elements. The full thermodynamic consistency of the constitutive model is discussed and extensively demonstrated regarding both, the pre-peak and post-peak regimes of the material response. Then the localization tensor is formulated and based on this, the performance of the localization indicator in the form of discontinuous bifurcation is numerically evaluated. The main objective is the evaluation of the sensitivity of the concrete material failure form with the content of recycled aggregates. The results in this paper demonstrate the capabilities of the proposed model to reproduce failure behaviors of RAC under arbitrary stress states recycled aggregate contents. The localization analyses demonstrate, particularly in plane stress conditions, that the addition of recycled aggregated does strongly increase the potentials for discontinuous failure modes. This is observed not only under uniaxial tensile and compressive stress conditions, but also under biaxial stresses. The content of recycled aggregates also affects the critical direction for localization which is a very important result. Finally, it is demonstrated in this paper that the effect of the recycled aggregated content on the failure mode and the critical direction for localized failure is much less significant in case of plane strain conditions.

2. Thermodynamics

2.1. First Law of Thermodynamics

The First Law of Thermodynamics states the balance equation between internal energy rate \dot{E} , the kinetic energy rate \dot{K} , the mechanic work of external forces P and the externally supplied heat Q , i.e.,

$$\dot{E} + \dot{K} = P + Q \quad (1)$$

with

$$\dot{E} = \int_{\Omega} \rho \dot{e} d\Omega; \quad \dot{K} = \frac{1}{2} \int_{\Omega} \rho \dot{\mathbf{u}} \cdot \dot{\mathbf{u}} d\Omega \quad (2)$$

$$P = \int_{\partial\Omega} \boldsymbol{\sigma} \cdot \mathbf{n} \cdot \dot{\mathbf{u}} d\Omega + \int_{\Omega} \rho \mathbf{b} \cdot \dot{\mathbf{u}} d\Omega \quad (3)$$

$$Q = \int_{\Omega} \rho r d\Omega - \int_{\partial\Omega} \mathbf{h} \cdot \mathbf{n} d\Omega \quad (4)$$

being e the internal energy density, ρ the material density and \mathbf{u} the velocity vector. Regarding the other terms, $\boldsymbol{\sigma}$ is the Cauchy stress tensor, \mathbf{b} the body forces vector, r the applied heat sources, and \mathbf{h} the heat flux vector. The above equations are formulated for an arbitrary material portion of continuum, occupying the volume Ω with the contour $\partial\Omega$ and the normal unitary vector \mathbf{n} .

By introducing Eqs. (2)–(4) in Eq. (1), applying the Gauss's theorem to transform the surface integral of Eq. (3) into a volumetric one, taking into account infinitesimal strains and null body (and inertial) forces and assuming that Eq. (1) holds for any arbitrary part of Ω , the explicit form of the internal energy density can be expressed as

$$\rho \dot{e} = \boldsymbol{\sigma} : \dot{\boldsymbol{\varepsilon}} + \rho r - \nabla \cdot \mathbf{h} \quad (5)$$

where $\boldsymbol{\varepsilon}$ is the infinitesimal strain tensor.

2.2. Second Law of Thermodynamics

The Second Law of Thermodynamics states that the amount of energy that can be efficiently converted into mechanical work irreversibly decreases, i.e.,

$$\dot{S} - Q_T \geq 0 \quad (6)$$

where \dot{S} represents the system entropy rate and Q_T the entropy flux, both defined as

$$\dot{S} = \int_{\Omega} \rho \dot{s} d\Omega \quad (7)$$

$$Q_T = - \int_{\partial\Omega} \frac{\mathbf{h} \cdot \mathbf{n}_s}{T} d\Omega + \int_{\Omega} \frac{\rho r}{T} d\Omega \quad (8)$$

being s the internal entropy density and T the absolute temperature. By replacing Eqs. (7) and (8) into Eq. (6) the weak form of the Second Law of Thermodynamic is obtained as

$$\int_{\Omega} \left[\rho \dot{s} + \nabla \cdot \left(\frac{\mathbf{h}}{T} \right) - \frac{\rho r}{T} \right] d\Omega \geq 0. \quad (9)$$

The general form of the Clausius-Duhem inequality (CDI) for porous media may be obtained by combining Eqs. (5) and (9) as

$$\int_{\Omega} \left(\boldsymbol{\sigma} : \dot{\boldsymbol{\varepsilon}} + \rho T \dot{s} - \rho \dot{e} - \frac{\mathbf{h}}{T} \cdot \nabla T \right) d\Omega \geq 0. \quad (10)$$

2.3. Thermodynamics of gradient-based poroplastic materials

In this section the Thermodynamics laws previously presented are considered to formulate and derive the thermodynamically consistent expressions of the constitutive equations for gradient-based poroplastic continua as considered for the modeling of RAC. Based on the original proposal by Simo and Miehe [30] for local inelastic media and its extension for gradient plasticity and small strain kinematics by Svedberg and Runesson [31] and Vrech and Etse [22], arbitrary thermodynamic states of thermodynamically consistent gradient-regularized materials may be defined in terms of the elastic strain tensor $\boldsymbol{\varepsilon}^e$, the elastic entropy s^e , the internal variables q and their spatial gradients ∇q . Therefore, the internal energy density can be expressed as

$$e = e(\boldsymbol{\varepsilon}^e, s^e, q, \nabla q). \quad (11)$$

By replacing the time derivative of Eq. (11) into Eq. (10), and considering that total strain and entropy are additively decomposed in their elastic and plastic parts, i.e., $\boldsymbol{\varepsilon}^e = \boldsymbol{\varepsilon} - \boldsymbol{\varepsilon}^p$ and $s^e = s - s^p$, the weak form of the Clausius-Duhem inequality results

$$\int_{\Omega} \left[\left(\boldsymbol{\sigma} - \rho \frac{\partial e}{\partial \boldsymbol{\varepsilon}^e} \right) : \dot{\boldsymbol{\varepsilon}} + \rho \left(T - \frac{\partial e}{\partial s^e} \right) \dot{s} + \rho \frac{\partial e}{\partial \boldsymbol{\varepsilon}^e} : \dot{\boldsymbol{\varepsilon}}^p + \rho \frac{\partial e}{\partial s^e} \dot{s}^p + \frac{\partial e}{\partial q} \dot{q} + \frac{\partial e}{\partial \nabla q} \cdot \nabla \dot{q} - \frac{\mathbf{h} \cdot \nabla T}{T} \right] d\Omega \geq 0 \quad (12)$$

Then, under consideration of the decomposition of the free energy density in the form $\psi = e - Ts$, and integrating by parts the gradient term $\int_{\Omega} \left(\frac{\partial \psi}{\partial \nabla q} \nabla \dot{q} \right) d\Omega$, Eq. (12) becomes

$$\int_{\Omega} \left[\left(\boldsymbol{\sigma} - \rho \frac{\partial \psi}{\partial \boldsymbol{\varepsilon}^e} \right) : \dot{\boldsymbol{\varepsilon}} + \rho \left(s + \frac{\partial \psi}{\partial T} \right) \dot{T} + \rho \frac{\partial \psi}{\partial \boldsymbol{\varepsilon}^e} : \dot{\boldsymbol{\varepsilon}}^p + Q_R \dot{q} - \frac{\mathbf{h} \cdot \nabla T}{T} \right] d\Omega + \int_{\partial\Omega} Q^{(b)} \dot{q} d\Omega \geq 0 \quad (13)$$

where $Q_R = Q_R^l + Q_R^g$, with Q_R^l and Q_R^g the local and gradient dissipative stresses in the domain Ω , which are defined as

$$Q_R^l = -\rho \frac{\partial \psi}{\partial q}; \quad Q_R^g = T \nabla \cdot \left(\frac{\rho}{T} \frac{\partial \psi}{\partial \nabla q} \right) \quad (14)$$

On the other hand, due to the existence of gradient terms, another dissipative stress $Q^{(b)}$ appears on the boundary $\partial\Omega$, which is obtained as

$$Q^{(b)} = -\mathbf{n}_s \cdot \rho \frac{\partial \psi}{\partial \nabla q}. \quad (15)$$

Finally, the Coleman's equations, and the plastic and thermal dissipations are defined as follows

$$\boldsymbol{\sigma} = \rho \frac{\partial \psi}{\partial \boldsymbol{\varepsilon}^e}; \quad s = -\frac{\partial \psi}{\partial T} \quad (16)$$

$$\varphi^p = \boldsymbol{\sigma} : \dot{\boldsymbol{\varepsilon}}^p + Q_R \dot{q}; \quad \varphi^{th} = -\frac{\mathbf{h} \cdot \nabla T}{T}. \quad (17)$$

In the following, the uncoupled expression of the total Helmholtz's free energy density is adopted for gradient-based elastoplastic materials

$$\psi(\boldsymbol{\varepsilon}^e, q, \nabla q) = \psi^e(\boldsymbol{\varepsilon}^e) + \psi^l(q) + \psi^g(\nabla q) \quad (18)$$

whereby ψ^e represents the elastic free energy, ψ^l the local plastic energy and ψ^g the gradient one. The elastic term of the Helmholtz's free energy under isothermal conditions is defined as

$$\rho \psi^e = \frac{1}{2} \boldsymbol{\varepsilon}^e : \mathbf{C} : \boldsymbol{\varepsilon}^e, \quad (19)$$

being \mathbf{C} the fourth order elastic tensor. The local plastic Helmholtz's free energy component turns

$$\rho \psi^l = \frac{H^l}{2} q^2, \quad (20)$$

which represents the so-called frozen free energy, since it is unrecovered after restoring the initial stress state. Regarding gradient-based materials, the non local free energy may be assumed as

$$\rho \psi^g = \frac{1}{2} l_c^2 H^g \nabla \cdot \nabla q \quad (21)$$

being H^l the local-plastic hardening/softening modulus, H^g the gradient softening modulus and l_c the gradient characteristic length. $Q^{(b)}$ can be described by means of a simple constitutive relation as

$$Q^{(b)} = c q \quad \text{with} \quad \bar{c} = H^g l_c \quad (22)$$

being $c \geq 0$ a non-dimensional scalar constant. In the present thermodynamically consistent formulation of gradient-plasticity, and similarly to previous works by Pamin [32], Svedberg and Runesson [31] and Vrech and Etse [22], it is chosen $c = 0$.

2.4. Constitutive equations

From Eqs. (16) and (19), the Cauchy stress tensor can be derived in terms of the elastic strain tensor as

$$\boldsymbol{\sigma} = \mathbf{C} : \boldsymbol{\varepsilon}^e \quad (23)$$

whereas, from Eqs. (14), (20) and (21) and after some algebra, the thermodynamically consistent local and non-local dissipative stresses result

$$\mathbf{Q}_R^l = -H^l \mathbf{q}, \quad \mathbf{Q}_R^g = l_c^2 H^g \nabla^2 \mathbf{q} \quad (24)$$

being ∇^2 the Laplacian operator.

2.5. Non-local poroplastic flow rule

By proceeding in the same way as for local plasticity, the rates of the plastic strain tensor and the internal variables are derived from the general non-associated flow rule and the dissipative potential Φ^* as follows

$$\dot{\boldsymbol{\varepsilon}}^p = \dot{\lambda} \frac{\partial \Phi^*}{\partial \boldsymbol{\sigma}}, \quad \dot{\mathbf{q}} = \dot{\lambda} \frac{\partial \Phi^*}{\partial \mathbf{Q}_R} \quad (25)$$

where $\dot{\lambda}$ is the rate of the plastic multiplier. To complete the constitutive formulation, the Kuhn-Tucker conditions are introduced

$$\dot{\lambda} \geq 0, \quad \Phi(\boldsymbol{\sigma}, \mathbf{Q}_R) \leq 0, \quad \dot{\lambda} \Phi(\boldsymbol{\sigma}, \mathbf{Q}_R) = 0 \quad (26)$$

being Φ the yield surface or loading function.

2.6. Gradient-based plastic consistency

Given the loading function Φ , the consistency condition for gradient-based plastic materials leads to

$$\dot{\Phi} = \frac{\partial \Phi}{\partial \boldsymbol{\sigma}} : \dot{\boldsymbol{\sigma}} + \frac{\partial \Phi}{\partial \mathbf{Q}_R} : \dot{\mathbf{Q}}_R \quad (27)$$

From Eq. (27) and regarding Eqs. (23)–(25), the following differential equation for the plastic multiplier is obtained

$$h \dot{\lambda} + \dot{\Phi}^{trial} + \dot{\Phi}^g = 0 \quad (28)$$

where h is the generalized local plastic modulus. The terms $\dot{\Phi}^{trial}$ and $\dot{\Phi}^g$ are the rates of the local and gradient loading functions, respectively. These values are defined as

$$h = -\frac{\partial \Phi}{\partial \boldsymbol{\sigma}} : \mathbf{C} : \frac{\partial \Phi^*}{\partial \boldsymbol{\sigma}} - H^l \frac{\partial \Phi}{\partial \mathbf{Q}_R} \frac{\partial \Phi^*}{\partial \mathbf{Q}_R} \quad (29)$$

$$\dot{\Phi}^{trial} = -\frac{\partial \Phi}{\partial \boldsymbol{\sigma}} : \mathbf{C} : \dot{\boldsymbol{\varepsilon}} \quad (30)$$

$$\dot{\Phi}^g = l_c^2 H^g \frac{\partial \Phi}{\partial \mathbf{Q}_R} \frac{\partial \Phi^*}{\partial \mathbf{Q}_R} \nabla^2 \dot{\lambda} \quad (31)$$

Taking into account Eqs. (25) and (28) and that $\boldsymbol{\varepsilon}^e = \boldsymbol{\varepsilon} - \boldsymbol{\varepsilon}^p$, Eq. (23) can be rewritten as

$$\dot{\boldsymbol{\sigma}} = \mathbf{C}^{ep} : \dot{\boldsymbol{\varepsilon}} + \mathbf{C}^g : \dot{\boldsymbol{\varepsilon}}^g \quad (32)$$

with the fourth-order elastoplastic constitutive tensor

$$\mathbf{C}^{ep} = \mathbf{C} - \frac{1}{h} \left(\mathbf{C} : \frac{\partial \Phi^*}{\partial \boldsymbol{\sigma}} \otimes \frac{\partial \Phi}{\partial \boldsymbol{\sigma}} : \mathbf{C} \right), \quad (33)$$

and the second-order gradient constitutive tensor

$$\mathbf{C}^g = -\frac{1}{h} \mathbf{C} : \frac{\partial \Phi^*}{\partial \boldsymbol{\sigma}} \quad (34)$$

3. Thermodynamically consistent constitutive model for recycled aggregate concrete

In this section the constitutive equations for RAC are formulated in the framework of the Second Law of Thermodynamic. Firstly, the maximum strength criterion is defined in terms of dissipative stresses in pre- and post-peak regimes. Then, the hardening and softening rules are formulated which provide thermodynamically consistency to the pre- and post-peak dissipative stresses. Despite the constraints involved in the thermodynamic framework of this constitutive theory formulation, it will be shown that the proposed model accounts for the fundamental complexities and parameters of RAC mechanical behavior and, therefore, is able to realistically predict its failure behavior.

3.1. Maximum strength criterion and plastic potential for RAC

The Leon-Drucker-Prager (LDP) strength criterion originally developed by Vrech and Etse [22], is extended in this formulation to account for the recycled aggregate content in the concrete mixture. The resulting expression of the RAC failure criterion takes the form

$$\Phi = \frac{3}{2} \beta_R {}^* \tau^2 + \gamma_R m_0 \left(\frac{{}^* \tau}{\sqrt{6}} + {}^* \sigma \right) - c_0 = 0 \quad (35)$$

in terms of the Haigh-Westergaard stress coordinates

$${}^* \sigma = \frac{I_1}{3f_c}, \quad {}^* \tau = \frac{\sqrt{2J_2}}{f_c} \quad (36)$$

being f_c the uniaxial compression strength, I_1 the first invariant of the normal stresses, and J_2 the second invariant of the deviatoric stresses, while $c_0 = 1$ and $m_0 = 3(f_c^2 - f_t^2)/(2f_c f_t)$. The influence of the recycled aggregate content is introduced through the parameters β_R and γ_R , computed as

$$\beta_R = \frac{1}{\alpha_R^2}; \quad \gamma_R = \frac{1}{\alpha_R}, \quad (37)$$

which, in turn, are functions of the so-called *concrete mixture recycling factor* α_R , defined as

$$\alpha_R = 1 - \alpha_1 (RA)^{\alpha_2} = \frac{f_c^R}{f_c} \quad \text{being } 0 < \alpha_R \leq 1, \quad (38)$$

where RA is the recycled aggregate ratio and, f_c and f_c^R are the peak strength in the uniaxial compression test for NAC and RAC, respectively. The coefficients α_1 and α_2 are positive values to be experimentally calibrated. Fig. 1 demonstrates the accuracy of the RAC-LDP constitutive model compared with the experimental data by Folino and Xargay [8].

In order to clarify the physics behind the influence of the RA content over the original LDP model, Eq. (35) may be rewritten in terms of the recycled aggregate-dependent cohesive and frictional parameters c_R and m_R . It can be easily seen that the higher the RA content, the lower the concrete mixture recycling factor α_R , and vice versa. This means, see Eqs. (40), that concrete loses cohesion and frictional capabilities under increasing contents of recycled aggregates. Moreover, the loss of cohesion is more drastic than the frictional one (note that $c_R < c_0$ and $m_R < m_0$, being c_0 and m_0 the cohesion and friction parameters of NAC). In fact, the typical mortar-to-mortar interfaces which turn evident in concretes with recycled aggregates is the most relevant cause behind the strong

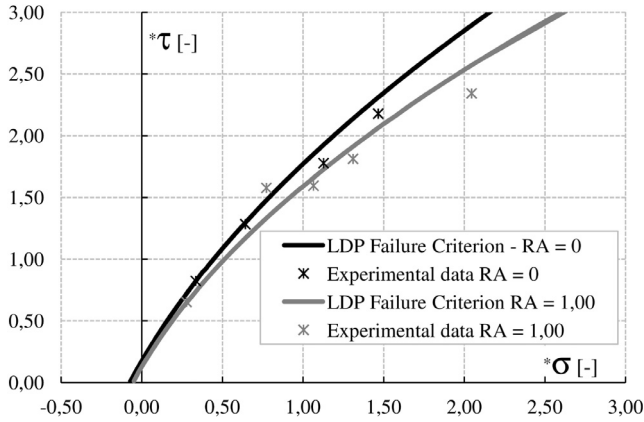


Fig. 1. Comparison of the RAC-LDP model against experimental data in compressive regime by Folino and Xargay [8].

loss of cohesion of RAC as compared to NAC (see Lima et al. [7] and Silva et al. [33]).

$$\Phi = \frac{3}{2} {}^* \tau^2 + m_R \left(\frac{{}^* \tau}{\sqrt{6}} + {}^* \sigma \right) - c_R = 0 \quad (39)$$

with

$$c_R = \alpha_R^2 c_0, \quad m_R = \alpha_R m_0 \quad (40)$$

The recycled aggregate dependent yield surface of the LDP model is also reformulated as

$$\Phi = \frac{3}{2} \beta_R {}^* \tau^2 + \gamma_R m_0 \left(\frac{{}^* \tau}{\sqrt{6}} + {}^* \sigma \right) - Q_R = 0 \quad (41)$$

with Q_R the dissipative stresses which eventually turns into ${}^h Q_R$ or ${}^s Q_R$ depending on whether the material is in hardening or softening regime, respectively. As it is well known, the lateral inelastic deformation of normal concrete increases as the confining pressure decreases. In case of RAC, the experimental evidence shows that this inelastic lateral strain in the low confinement regime more significantly increases with the recycled aggregate content [8]. To account for this fundamental effect, a volumetric and recycled aggregate content-dependent plastic potential is proposed as follows

$$\Phi^* = \frac{3}{2} \beta_R {}^* \tau^2 + \gamma_R m_0 \left(\frac{{}^* \tau}{\sqrt{6}} + \eta_R {}^* \sigma \right) - Q_R = 0 \quad (42)$$

being η_R the degree of volumetric non-associativity defined in terms of the confining pressure and recycled aggregate content as

$$\eta_R = \eta - (1 - \eta) \exp[\alpha_R ({}^* \sigma - {}^* \sigma_0) - 1]. \quad (43)$$

Thereby, η is the minimum value of the degree of volumetric non-associativity which is obtained on the edge of the plastic potential, where it intersects the hydrostatic axis. At this stress state the normalized form of the effective first stress coordinate approaches its maximum value ${}^* \sigma = {}^* \sigma_0$. Note that, η decreases with increasing RA content, leading to the increment of the non-associativity degree in case of RAC.

3.2. Thermodynamically consistent hardening rule for RAC

Concrete stiffness in pre-peak regime is one of the most affected mechanical features due to the presence of recycled aggregates.

In the proposed RAC-LDP model, the inelastic local free energy density controlling the hardening response of RAC material is defined as

$$\rho {}^h \psi = -{}^h Q_0 {}^h q + \frac{0.9}{\chi_h} \cos(\chi_h {}^h q) \quad (44)$$

As demonstrated by Li et al. [34], the ductility reduction of RAC in pre-peak regime is another relevant aspect as compare to NAC mechanical behavior. In the present model formulation, this effect is taken into account through the recycled aggregate content-dependent ductility measure in hardening

$$\chi_h = -\frac{\pi}{2} \frac{\|\boldsymbol{\varepsilon}^p\|}{x_R} \quad (45)$$

being $\|\boldsymbol{\varepsilon}^p\|$ the equivalent plastic strain and x_R the hardening ductility measure which decreases with the RA content leading a more ductile behavior of RAC in comparison with NAC, and which is defined as a function of the normalized confining pressure and the concrete mixture recycling factor as

$$x_R = \alpha_R A_h \exp(B_h {}^* \sigma'). \quad (46)$$

The coefficients A_h and B_h must be experimentally calibrated. The expression of the hardening dissipative stress ${}^h Q_R$ is obtained from Eqs. (44) and (45) as

$${}^h Q_R = -\rho \frac{\partial {}^h \psi}{\partial {}^h q} = {}^h Q_0 + 0.9 \sin(\chi_h {}^h q), \quad (47)$$

where ${}^h Q_0 = 0, 10$ and ${}^h q$ represents the scalar hardening variable obtained from Eqs. (25) and (42) as

$${}^h \dot{q} = \dot{\lambda} \frac{\partial \Phi^*}{\partial {}^h Q_R} = -\dot{\lambda}. \quad (48)$$

From Eqs. (47) and (48) the recycled aggregate dependent hardening evolution law is obtained as

$${}^h \dot{Q}_R = -\rho \frac{\partial^2 {}^h \psi}{(\partial {}^h q)^2} {}^h \dot{q} \rightarrow {}^h \dot{Q}_R = {}^h H_R^l \dot{\lambda} \quad (49)$$

with the hardening plastic modulus for RAC

$${}^h H_R^l = \rho \frac{\partial^2 {}^h \psi^l}{(\partial {}^h q)^2} = -0.9 \chi_h \cos(\chi_h {}^h q). \quad (50)$$

3.3. Thermodynamically consistent softening rule for RAC

This model formulation considers that the energy dissipation in the post-peak regime is due to two uncoupled mechanisms: a local or fracture energy based one, and a non-local gradient one. Thus, the free energy density of the RAC-LDP model in softening can be additively decomposed as ${}^s \psi = {}^s \psi^f + {}^s \psi^g$, being ${}^s \psi^f$ the local free energy density component and ${}^s \psi^g$ the non-local one.

According to the fracture energy based plasticity model by Willam and Etse [35], the local free energy density in softening can be defined as

$${}^s \psi^f = -\frac{1}{\rho \alpha_f} \exp(\alpha_f {}^s q) \quad (51)$$

being ${}^s q$ the scalar softening variable. The local or fracture energy based dissipative stress Q_R^f can be derived from Eqs. (14) and (51) as

$$Q_R^f = -\rho \frac{\partial {}^s \psi^f}{\partial {}^s q} = \exp(\alpha_f {}^s q) \quad (52)$$

with

$$\alpha_f = 5 \frac{h_f}{u_R} \|\langle \boldsymbol{\varepsilon}_f \rangle\| \quad (53)$$

being $\boldsymbol{\varepsilon}_f$ the local fracture strain. The Mc Auley brackets indicate that only the tensile plastic strains contribute to the energy density during the fracture process. Then, u_R represents the maximum crack opening displacement of RAC mode I type of failure which is defined in terms of the concrete mixture recycling factor as

$$u_R = \alpha_R u_r \quad (54)$$

with u_r the maximum crack opening displacement of the associated NAC, which is obtained when $\alpha_R \rightarrow 1$. The characteristic length h_f represents the distance between active macrocracks and it is defined as

$$h_f = \frac{h_t}{R_G} \quad (55)$$

with

$$R_G = \begin{cases} 1 & * \sigma \geq 0, \\ C_u + D_u \sin(2 * \sigma - \frac{\pi}{2}), & 0 \geq * \sigma \geq -1.5, \\ 100, & * \sigma \leq -1.5. \end{cases} \quad (56)$$

where C_u and D_u are constants to be experimentally calibrated and h_t is the characteristic length of the related NAC material in mode I type of fracture. In Eq. (56) R_G continuously increases under increasing confinement pressure $*\sigma$, leading to the reduction of the distance between macrocracks as represented by h_f in Eq. (55) and, consequently to a more diffused type of failure.

The presence of recycled aggregates only affects the fracture energy based strength degradation Q_R^f . This is because, the fracture energy is directly related to the mechanical properties of both the aggregates and the Interfacial Transition Zone (ITZ). The recycled aggregate dependent local softening evolution law can be obtained as

$$\dot{Q}_R^f = {}^s H_R^l \dot{\lambda}, \quad (57)$$

with the local softening plastic modulus computed as

$${}^s H_R^l = \rho \frac{\partial^2 \psi^l}{(\partial^s q)^2} = -\alpha_f \exp(\alpha_f {}^s q). \quad (58)$$

The gradient component of the inelastic free energy density is expressed in terms of the gradient of the scalar softening state variable $\nabla^s q$.

$${}^s \psi^g(\nabla^s q) = \frac{1}{2\rho} l_c^2 {}^s H^g \nabla^2 ({}^s q). \quad (59)$$

From Eq. (14-b), the non-local dissipative stress in softening results

$$Q^g = \nabla \cdot \rho \frac{\partial \psi^{nl}}{\partial (\nabla^s q)} = l_c^2 {}^s H^g \nabla^2 ({}^s q) \quad (60)$$

and its evolution law yields

$$\dot{Q}^g = -l_c^2 {}^s H^g \nabla^2 \dot{\lambda} \quad (61)$$

being H^g the non-local gradient modulus and l_c the gradient-based characteristic length defined in terms of the acting confinement as follows

$$l_c = \begin{cases} 0 & * \sigma \geq 0, \\ E_l l_m [1 + \sin(F_l * \sigma - \frac{\pi}{2})], & 0 \geq * \sigma \geq -1.5, \\ l_m, & -1.5 \geq * \sigma. \end{cases} \quad (62)$$

with l_m the maximum internal length and E_l and F_l the internal parameters that appropriately define the variation of l_c with the confining pressure.

Finally, the total dissipative stress in softening is obtained from the addition of Eqs. (52) and (60) as ${}^s Q_R = Q_R^f + Q^g$.

4. Localized failure condition of the RAC-LDP constitutive model

In quasi-brittle materials like concrete, material failure is given by a succession of events starting in a small scale, which leads to progressive deterioration of the continuous medium and turns it

into a discontinuum. This is characterized by strong spatial discontinuities of the kinematic fields [35,36].

In tensile regime the concrete response is highly brittle as the damage entirely localizes in one single crack while in compressive regime the ductility of concrete failure behavior strongly increases with the confining pressure, and it is governed by both, fracture energy releases in active microcracks and material degradation in between these cracks [9].

Several analytical and geometrical attempts have been aimed to capture the onset of localization and to determine both direction and amplitude of the related cracks or shear bands. In this sense, mathematical indicators that signalize the initiation of localized failure modes in the form of discontinuous bifurcation were performed in the field of quasi-brittle materials [37].

In solid continuous, discontinuities may occur in the spatial derivatives of the body velocity $\dot{\mathbf{z}} = \nabla \dot{\mathbf{u}}$. The jumps of the kinematic variables can be written as [38]

$$[[\dot{\mathbf{z}}]] = [[\nabla \dot{\mathbf{u}}]] = \mathbf{n} \otimes \mathbf{g} \quad (63)$$

with \mathbf{n} the normal of the discontinuity surface and \mathbf{g} the polarization vector. The balance of linear momentum across the discontinuity surface leads to the following localization condition [38]

$$c[[\nabla \cdot \boldsymbol{\sigma}]] + \mathbf{n} \cdot [[\dot{\boldsymbol{\sigma}}]] \doteq \mathbf{0}. \quad (64)$$

If a quasi-static problem is considered and neglecting inertial forces, the momentum balance equation yields $\nabla \cdot \boldsymbol{\sigma} = 0$. Finally Eq. (64) implies

$$\mathbf{n} \cdot [[\dot{\boldsymbol{\sigma}}]] \doteq \mathbf{0} \quad (65)$$

By considering an homogeneous state before the onset of discontinuous bifurcation, harmonic perturbations are applied to the incremental field variables; the displacements and the plastic multiplier, which represent the propagation of stationary planar waves. Then, the solutions of the field variables are expressed as

$$\begin{pmatrix} \dot{\mathbf{u}} \\ \dot{\lambda} \end{pmatrix} = \begin{pmatrix} \dot{U}(t) \\ \dot{L}(t) \end{pmatrix} \exp\left(\frac{i2\pi}{\delta} \mathbf{n} \cdot \mathbf{x}\right) \quad (66)$$

being \mathbf{x} the position vector and δ the wave length. The spatially homogeneous amplitudes of the wave solutions are represented by $\dot{U}(t)$ and $\dot{L}(t)$. By substituting Eq. (66) into Eq. (31), the following form of the non-local part of the plastic consistency is obtained

$$\dot{\Phi}^g = -h^g \dot{\lambda} \quad (67)$$

with the generalized gradient modulus as

$$h^g = l_c^2 H^g \frac{\partial \Phi}{\partial Q_R} \frac{\partial \Phi^*}{\partial Q_R} \left(\frac{2\pi}{\delta}\right)^2 \quad (68)$$

Taking into account Eqs. (67) and (68), then Eqs. (28) and (32) become

$$(h + h^g) \dot{\lambda} + \dot{\Phi}^{trial} = 0; \quad \dot{\boldsymbol{\sigma}} = \mathbf{C}_g^{ep} : \dot{\boldsymbol{\varepsilon}} \quad (69)$$

with

$$\mathbf{C}_g^{ep} = \mathbf{C} - \frac{1}{(h + h^g)} \left(\mathbf{C} : \frac{\partial \Phi^*}{\boldsymbol{\sigma}} \otimes \frac{\partial \Phi}{\boldsymbol{\sigma}} : \mathbf{C} \right). \quad (70)$$

By introducing Eqs. (69-b) and (70) in Eq. (65), the jump of the rate of the Cauchy tensor can be obtained in the non-local form as

$$\mathbf{n} \cdot [[\dot{\boldsymbol{\sigma}}]] = \mathbf{n} \cdot \mathbf{C}_g^{ep} : [[\dot{\boldsymbol{\varepsilon}}]] = \mathbf{Q}_g^{ep} \cdot \mathbf{g} \doteq \mathbf{0} \quad (71)$$

with the second-order gradient acoustic tensor

$$\mathbf{Q}_g^{ep} = \mathbf{Q}^E - \mathbf{n} \cdot \left[\frac{1}{(h + h^g)} \left(\mathbf{C} : \frac{\partial \Phi^*}{\boldsymbol{\sigma}} \otimes \frac{\partial \Phi}{\boldsymbol{\sigma}} : \mathbf{C} \right) \right] \cdot \mathbf{n} \quad (72)$$

where $\mathbf{Q}^E = \mathbf{n} \cdot \mathbf{C} \cdot \mathbf{n}$ is the second-order elastic acoustic tensor. Finally, localization of deformation takes place if Eq. (71) admits a solution for any polarization vector \mathbf{g} different to zero. Consequently, the following condition must be fulfilled

$$\det(\mathbf{Q}_g^{ep}) = 0. \tag{73}$$

Note that in case of local materials Eq. (72) becomes

$$\mathbf{Q}^{ep} = \mathbf{Q}^E - \mathbf{n} \cdot \left[\frac{1}{h} \left(\mathbf{C} : \frac{\partial \Phi^*}{\partial \boldsymbol{\sigma}} \otimes \frac{\partial \Phi}{\partial \boldsymbol{\sigma}} : \mathbf{C} \right) \right] \cdot \mathbf{n} \tag{74}$$

and therefore, the localization condition leads to

$$\det(\mathbf{Q}^{ep}) = 0. \tag{75}$$

5. Finite element analysis

In this section, the main features and capabilities of the proposed material model are studied by comparison of some numerical results against experimental data available in the literature. The dual mixed finite element (FE) formulation for thermodynamically consistent gradient plasticity proposed by Vrech and Etse [39] is considered in the computational analysis. This formulation is based on the original proposal by Svedberg and Runesson [31] for gradient-regularized plasticity coupled with damage, leading to a very stable numerical performance even in case of localized failure modes. Fig. 2 shows the FE discretization and the boundary conditions adopted in this work. The considered tests involve prismatic and cylindrical samples (specific dimensions are provided in the description of each test) under plane stress or cylindrical stress conditions, respectively. Two types of tests were selected to evaluate the predictive capabilities of the proposed model: uniaxial tensile and compression tests, which are very appropriate to analyze the soundness of the proposed constitutive theory. First, numerical analysis of the uniaxial tensile test by Akita et al. [40], performed on concrete prisms of 100 × 100 × 400 mm, are carried out. The fundamental material properties and model parameters used in the computational analysis are summarized in Tables 1 and 2.

Fig. 3 compares the model predictions and experimental data for uniaxial tensile tests performed on NAC and RAC with 100% content of recycled aggregates. It shows very good agreement regarding peak strength, post-peak behavior and residual strength, for both NAC and RAC cases. Next, numerical predictions of the uniaxial compression tests are studied under cylindrical stress conditions. These results are compared with experimental results by

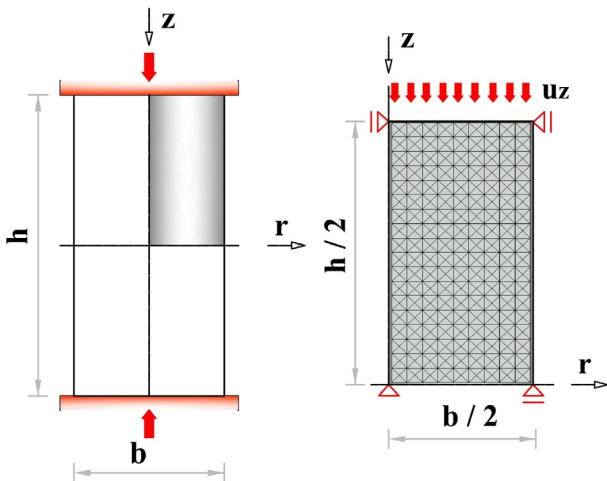


Fig. 2. FE discretization and boundary conditions.

Table 1
RAC-LDP model parameters.

Hardening law - $A_h; B_h$	0.002; -0.13 MPa ⁻¹
Gradient softening law - $E_f; F_f$	0.50; 2.00
Max. crack opening (Mode I) - u_r	0.127 mm
Max. gradient charact. length - l_m	70.00 mm
Maximum aggregate size - l_{ca}	18.00 mm
Gradient soft. parameter - ${}^s H^g$	1 MPa
Min. non-associative degree - η_0	0.30

Table 2
Concretes properties.

	Akita et al. [40]	Folino and Xargay [8]
E	11.00 GPa	31.67 GPa
f_c	22.50 MPa	36.52 MPa
f_t	2.50 MPa	4.04 MPa
α_{r1}	0.00055	0.00075
α_{r2}	1.05	1.25

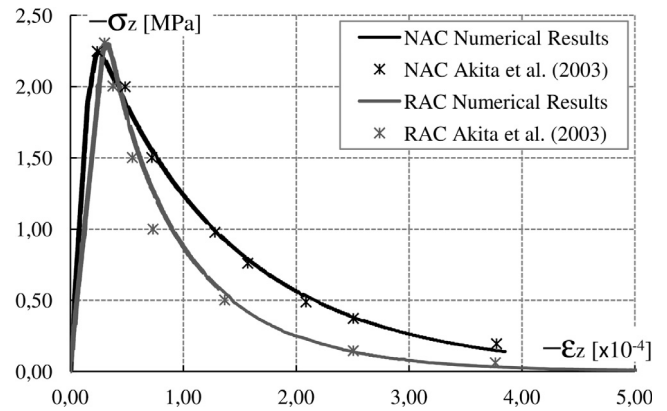


Fig. 3. Numerical results of uniaxial tensile tests against experimental results by Akita et al. [40].

Folino and Xargay [8] on concrete cylinders of 100 × 200 mm with different contents of recycled aggregates. The material properties used in these tests are shown in Table 2. Fig. 4 shows the predictions of the proposed model against the experimental data for NAC and RAC with 30%, 60% and 100% recycled aggregate contents. It also shows good agreement regarding both the pre-peak behavior and the peak strength for all different cases.

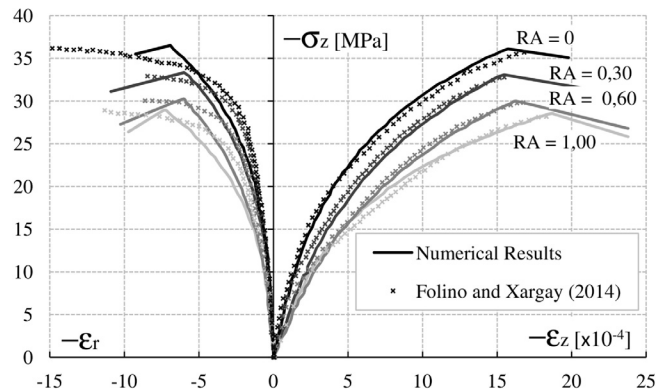


Fig. 4. Numerical results of uniaxial compression tests against experimental results by Folino and Xargay [8].

6. Localized failure analysis with the RAC-LDP model

To determine the influence of the recycled aggregate content in the occurrence of localized failure modes, the variations of the transition point from ductile to brittle failure mode as well as of the critical direction for discontinuous bifurcation are analyzed.

Hereinafter, the performance of the localized failure indicator is evaluated on the maximum strength surface of the gradient and fracture energy based model for RAC, under consideration of different stress conditions: (1) plane stress and (2) plane strain states. The components of the stress invariants fulfilling the maximum strength surface are obtained from Eq. (35), under consideration of a defined recycled aggregate content. For this localization analysis, the concrete properties by Folino and Xargay [8] and the model parameters listed in Tables 1 and 2 are used.

6.1. Plane stress condition

In this section, the failure localization analysis is performed for the particular case of $\sigma_3 = 0$, i.e., for plane stresses state. Next, the results of the numerical localization analysis are presented and discussed focusing on the effect of the recycled aggregate content on the performance of the localization indicator.

In first place, the variation of the normalized localization indicators $\det(\mathbf{Q}_g^{ep})/\det(\mathbf{Q}^E)$ and $\det(\mathbf{Q}^{ep})/\det(\mathbf{Q}^E)$ are shown along the maximal strength criterion defined in terms of the normalized principal stresses (σ_1/f_c ; σ_2/f_c) for four different recycled aggregate contents: $RA = 0, 0.30, 0.60$ and 1 , see Fig. 5 where the normalized localization indicator is represented as an ordinate in the normal direction to the corresponding maximum strength surface. Positive values are shown in the outward direction. The intersections between the maximum strength surfaces and the envelope of the segments representing the norm of the localization tensor signalizes the so-called transition point (TP) from ductile to brittle failure mode.

According to the results in Fig. 5, it can be concluded that, under plane stress condition, the material failure modes show very low dependency on the recycled aggregate content. This fact follows from the comparison between the length of the zones under localized failure with respect to the total perimeter of the failure surface, for each particular recycled aggregate content. This ratio remains practically invariant with the different recycled aggregate content. However, this conclusion does not mean that the critical direction for localization is independent of the recycled aggregate content. This property will be evaluated in the following. Next, the localization indicators $\det(\mathbf{Q}_g^{ep})$ and $\det(\mathbf{Q}^{ep})$ normalized respect to $\det(\mathbf{Q}^E)$ are numerically evaluated at the peak stresses to the uniaxial compression ($\sigma_1 < 0, \sigma_2 = 0$), biaxial compression ($\sigma_2 = 0.6\sigma_1$), pure shear ($\sigma_1 = -\sigma_2$) and uniaxial tensile tests ($\sigma_1 > 0, \sigma_2 = 0$) under plane stress conditions with different recycled aggregate contents. This is shown in Figs. 6–9. Two different forms of the proposed constitutive equations are considered. On the one hand, full local version of the proposed model, which is obtained by suppressing the gradient terms in the softening rule. On the other hand, gradient and fracture energy based formulation which includes both the fracture energy based and the gradient plasticity based contributions to the post-peak strength. Once again, four recycled aggregate contents are considered in the localization analysis: 0%, 30%, 60% and 100%.

From the results in Figs. 6 and 7 can be concluded that the local form of the proposed formulation is unable to suppress discontinuous bifurcation at peak stress of the different considered tests. Contrarily, the gradient non-local model lead to diffuse failure form as the uniqueness condition is satisfied.

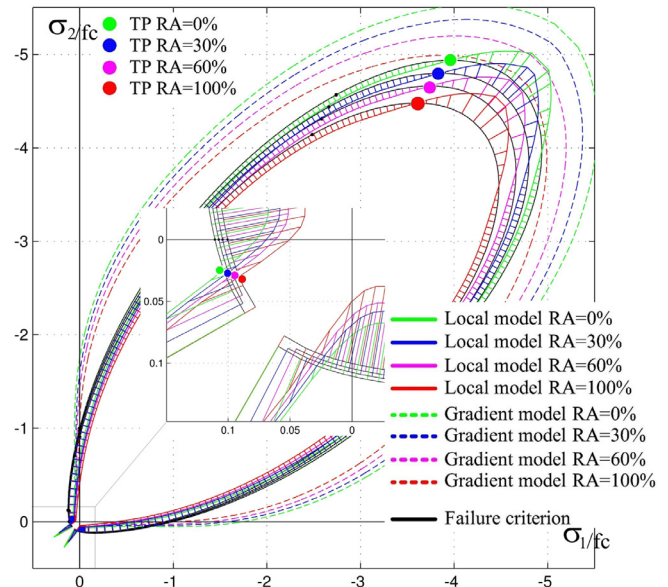


Fig. 5. Normalized localization indicators drawn in normal direction to the RAC-LDP maximum strength criterion under plane stress state.

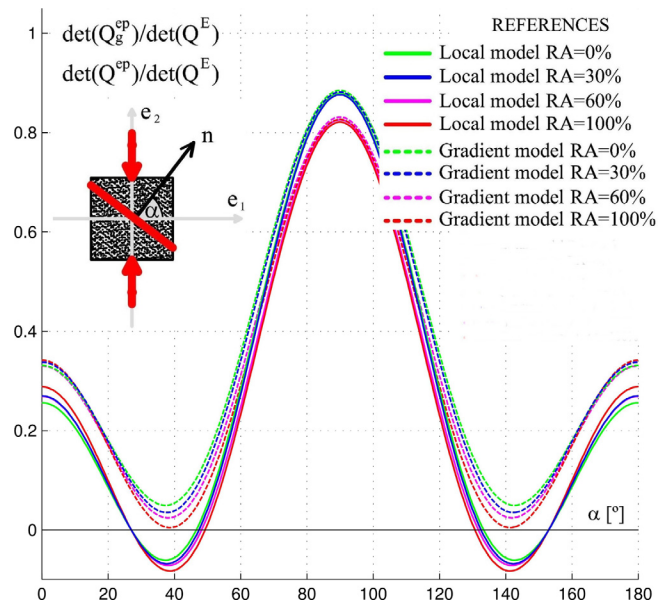


Fig. 6. Failure localization analysis at the peak of the uniaxial compression test under plane stress state.

In case of the pure shear and the uniaxial tensile tests, due to the fact that the first invariant of the involved stress states (in case of plane stress condition) turns zero, then the gradient characteristic length as defined in this formulation approaches also zero. Consequently, the regularization capabilities of the non-local component disappears. Consequently, the performance of the localization indicator of the local and full non-local models in Figs. 8 and 9 fully agree and indicate the existence of localized failure modes.

Finally, the results in Figs. 6–9 indicate that the critical directions for localization are affected by the recycled aggregate content. These critical directions are summarized in Table 3. It can be observed that for increasing recycled aggregate content, the critical localization angles corresponding to the peak stresses of

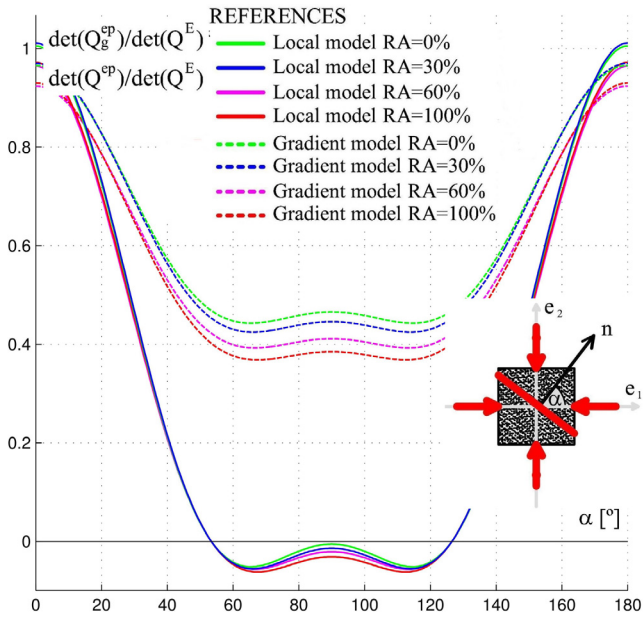


Fig. 7. Failure localization analysis at the peak of the biaxial compression test under plane stress state.

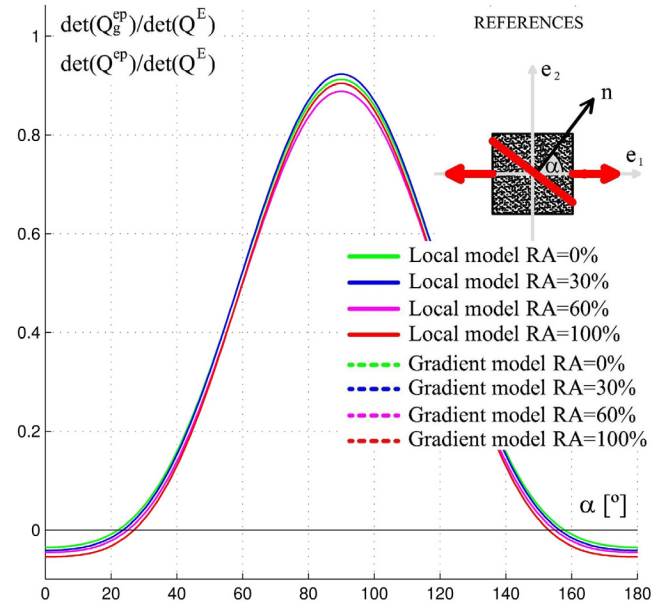


Fig. 9. Failure localization analysis at the peak of the uniaxial tensile test under plane stress state.

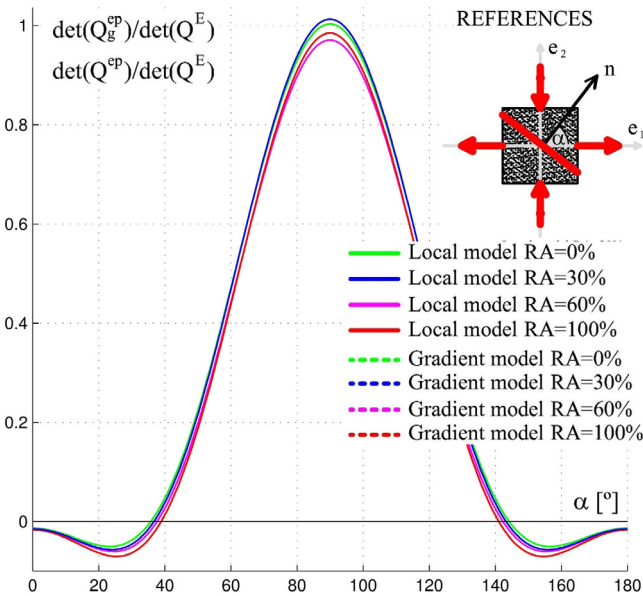


Fig. 8. Failure localization analysis at the peak of the pure shear test under plane stress state.

the uniaxial compression, biaxial compression and pure shear tests, increase their inclinations. This means that the microcracks move to the horizontal direction with higher recycled aggregate contents.

6.2. Plane strain condition

In this section, the localization analysis of the thermodynamically consistent RAC-LDP constitutive model considers the particular case of plane strain conditions, when $\sigma_3 = \nu(\sigma_1 + \sigma_2)$.

As first step, the relationships $\det(Q_g^{ep})/\det(Q^E)$ and $\det(Q^{ep})/\det(Q^E)$ are shown in terms of the normalized principal stresses (σ_1/f_c ; σ_2/f_c) for four different recycled aggregate contents: 0,

Table 3 Critical localization angles in plane stress state. PS: pure shear, UT: uniaxial tension, UC: uniaxial compression, BC: biaxial compression.

RA [%]	Critical localization angle [°]			
	PS	UT	UC	BC
0	23.62	0	37.13	62.25
30	24.19	0	37.69	65.81
60	24.75	0	38.25	66.94
100	25.31	0	38.81	67.50

0.30, 0.60 and 1, see Fig. 10. For lower recycled aggregate contents, the material behaves very stable in almost all the stress domain and there is evidence of discontinuous bifurcation only very close to the apex, while for higher recycled aggregate contents, localized failure modes are a little bit more evident.

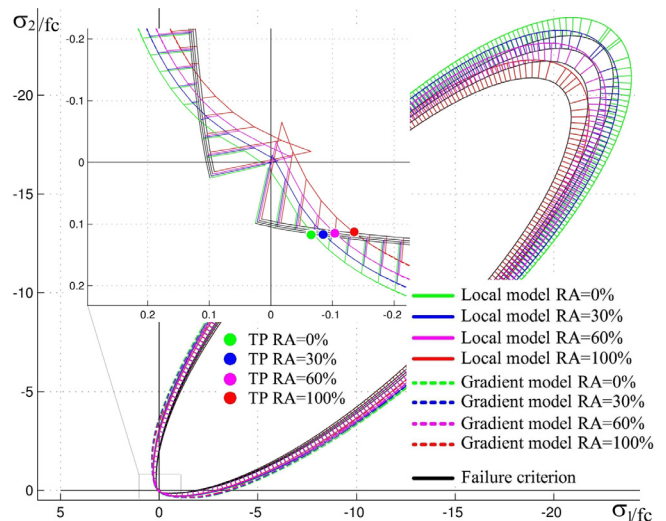


Fig. 10. Normalized localization indicators drawn in normal direction to the extended LDP maximum strength criterion under plane strain state.

In contrast to the plane stress state, the transitions points appear in zones of very low confinement. This means that the plane strain condition as compare to the plane stress one is related to more stable failure modes all along the failure surface. In Figs. 11–14, the results of the normalized localization indicators $\det(Q_g^{ep})/\det(Q^E)$ and $\det(Q^{ep})/\det(Q^E)$ are shown in orthogonal coordinates, being numerically evaluated at peak stresses of the uniaxial compression, biaxial compression ($\sigma_2 = 0.6\sigma_1$), pure shear and uniaxial tensile tests under plane strain conditions and for different recycled aggregate contents. These results demonstrate the absence of discontinuous bifurcation in almost all peak stress conditions in consideration. Discontinuous bifurcation happens only for the highest recycled aggregate content (100%), under uniaxial tensile conditions. It can be also observed from the obtained numerical results, that in the uniaxial compression and pure shear

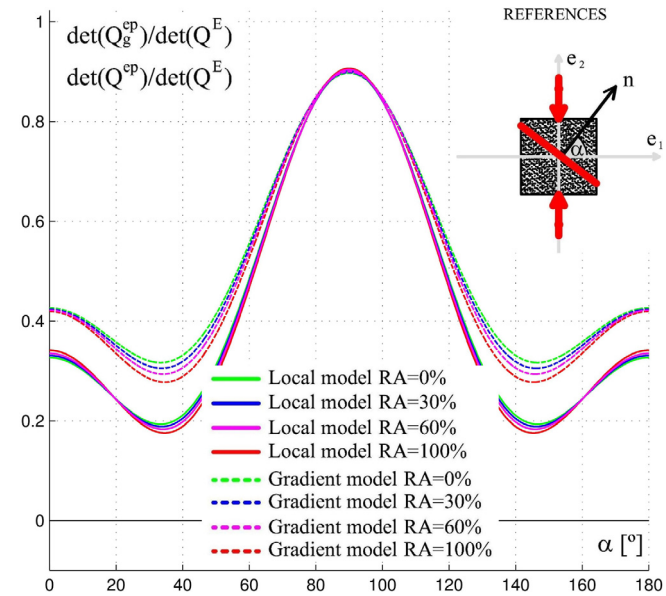


Fig. 11. Failure localization analysis at the peak of the uniaxial compression test under plane strain state.

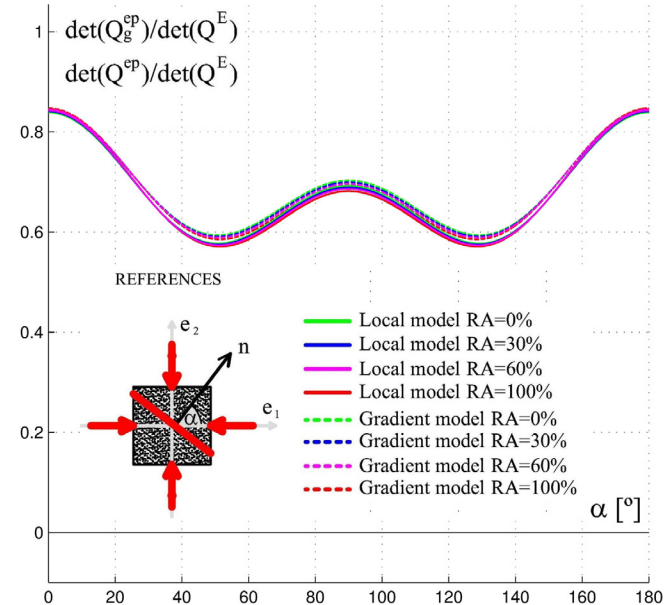


Fig. 12. Failure localization analysis at the peak of the biaxial compression test under plane strain state.

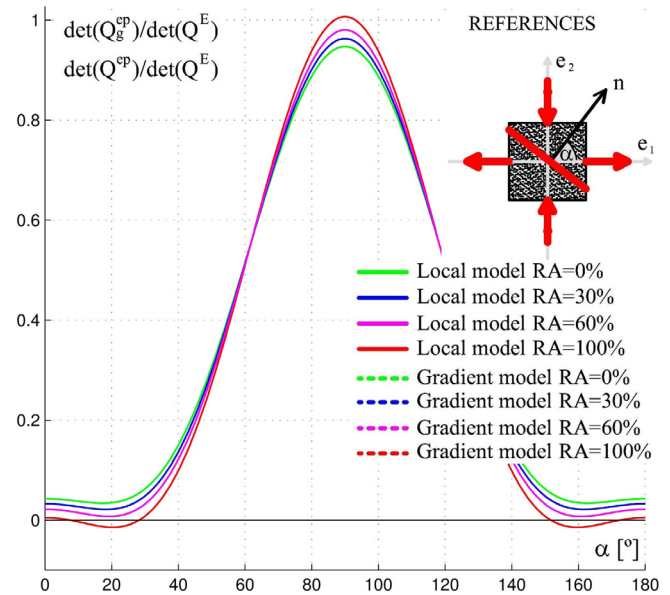


Fig. 13. Failure localization analysis at the peak of the pure shear test under plane strain state.

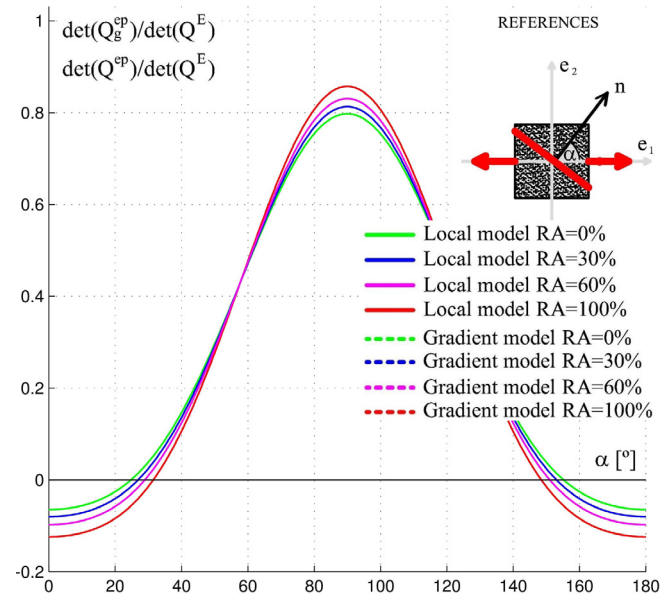


Fig. 14. Failure localization analysis at the peak of the uniaxial tensile test under plane strain state.

tests, the inclination angle of the critical direction for localized failure increases with the recycled aggregate content. But it does not depend on the recycled aggregate content in case of the uniaxial tensile test, as can be observed in Table 4.

Table 4
Critical localization angles in plane strain state. PS: pure shear, UT: uniaxial tension, UC: uniaxial compression, BC: biaxial compression.

RA [%]	Critical localization angle [°]			
	PS	UT	UC	BC
0	17.34	0	33.42	50.82
30	18.30	0	33.78	51.00
60	19.20	0	34.14	51.18
100	20.34	0	34.62	51.42

7. Conclusions

In this work, a thermodynamically consistent gradient-based constitutive theory was extended to simulate the failure behavior of RAC composed by arbitrary recycled aggregate contents. The main features of RAC as compared to NAC are taken into account by means of consistent reformulations of the maximum strength criterion, the hardening law and the fracture-energy based softening law of the constitutive model in terms of the so-called *concrete mixture recycling factor*. This parameter was also considered to reformulate the non-associated flow rule of the constitutive law to account for the larger plastic dilatancy of RAC in comparison to NAC.

The proposed constitutive model is able to capture the influence of the recycled aggregate content on the failure response behavior. In this regard, the analysis of the localization indicator, in terms of the determinant to the localization tensor, demonstrates that at peak stress of the all tests and stress states, the direction of the potential discontinuity surface is very sensitive to the recycled aggregate content and this sensitivity is larger under uniaxial compression and pure shear stress conditions than under uniaxial tensile stress state. The results also support the conclusion that the potentials for localized failure mode increase with the recycled aggregate content.

Acknowledgements

This study is part of the activities carried out by the authors within the EnCoRe project (www.encore-fp7.unisa.it), funded by the European Union within the Seventh Framework Programme (FP7-PEOPLE-2011-IRSES, n. 295283). The authors also acknowledge the financial support for this work by CONICET – Argentina (National Council for Science and Technology) through the Grant PIP 112-2011010-1079 and by CIUNT (Research council of the University of Tucuman) through the Grant 26/E-511.

References

- [1] NRMCA, National Ready Mixed Concrete Association. Concrete CO₂ fact sheet. MD: Silver Spring; 2012. p. 13 <<http://www.nrmca.org>>.
- [2] Li X. Recycling and reuse of waste concrete in China: Part II. Structural behaviour of recycled aggregate concrete and engineering applications. *Resour Conserv Recy* 2009;53(3):107–12.
- [3] Breccolotti M, Materazzi A. Structural reliability of eccentrically-loaded sections in RC columns made of recycled aggregate concrete. *Eng Struct* 2010;32(11):3704–12.
- [4] RILEM-TC-121-DRG. Specifications for concrete with recycled aggregates, vol. 27. Mater. Struct.; 1994.
- [5] NTC. Norme tecniche per le costruzioni (Italian Recommendations). 29; Decreto Ministeriale 14 gennaio; 2008.
- [6] Kou S, Poon C. Enhancing the durability properties of concrete prepared with coarse recycled aggregate. *Constr Build Mater* 2012;35:69–76.
- [7] Lima C, Caggiano A, Faella C, Martinelli E, Pepe M, Realfonzo R. Physical properties and mechanical behaviour of concrete made with recycled aggregates and fly ash. *Constr Build Mater* 2013;47:547–59.
- [8] Folino P, Xargay H. Recycled aggregate concrete-mechanical behavior under uniaxial and triaxial compression. *Constr Build Mater* 2014;56:21–31.
- [9] Etse G, Willam K. Fracture energy-based constitutive theory for inelastic behavior of plain concrete. *J Eng Mech* 1994;120(9):1983–2011.
- [10] Comi C, Perego U. Fracture energy based bi-dissipative damage model for concrete. *Int J Solids Struct* 2001;38(36–37):6427–54.
- [11] Bazant ZP, Oh B. Crack band theory for fracture concrete. *Mater Struct* 1983;16:155–77.
- [12] Oliver J. A consistent characteristic length for smeared cracking models. *J Numer Methods Eng* 1989;28:461–74.
- [13] Vardoulakis I, Aifantis EC. A gradient flow theory of plasticity for granular materials. *Acta Mech* 1991;87:197–217.
- [14] Comi C. A non-local model with tension and compression damage mechanisms. *Eur J Mech A/Solids* 2001;20(6–7):1–22.
- [15] Simone A, Wells G, Sluys L. From continuous to discontinuous failure in a gradient-enhanced continuum damage model. *Comput Methods Appl Mech Eng* 2003;192(41):4581–607.
- [16] Gao H, Huang Y, Nix WD, Hutchinson JW. Mechanism-based strain gradient plasticity - I. Theory. *J Mech Phys Solids* 1999;47:1239–63.
- [17] Abu Al-Rub RK, Voyiadjis GZ. Analytical and experimental determination of the material intrinsic length scale of strain gradient plasticity theory from micro- and nano-indentation experiments. *Int J Plast* 2004;20:753–82.
- [18] Abu Al-Rub RK, Voyiadjis GZ. A physically based gradient plasticity theory. *Int J Plast* 2006;22(4):654–84.
- [19] Peerlings R, de Borst R, Brekelmans W, Geers M. Gradient enhanced damage modelling of concrete fracture. *Mech Cohes-Frict Mater* 1998;3:323–42.
- [20] Pan Y, Wang X, Li Z. Analysis of the strain softening size effect for rock specimens based on shear strain gradient plasticity theory. *Int J Rock Mech Min Sci* 2002;39(6):801–5.
- [21] Peerlings R, Massart T, Geers M. A thermodynamically motivated implicit gradient damage framework and its application to brick masonry cracking. *Comput Methods Appl Mech Eng* 2004;193:3403–17.
- [22] Vrech S, Etse G. Gradient and fracture energy-based plasticity theory for quasi-brittle materials like concrete. *Comput Method Appl Mech* 2009;199(1–4):136–47.
- [23] Ripani M, Etse G, Vrech S, Mroginski J. Thermodynamic gradient-based poroplastic theory for concrete under high temperatures. *Int J Plast* 2014;61:157–77.
- [24] Poon C, Shui Z, Lam L. Effect of microstructure of ITZ on compressive strength of concrete prepared with recycled aggregates. *Constr Build Mater* 2004;18(6):461–8.
- [25] Corinaldesi V. Mechanical and elastic behaviour of concretes made of recycled concrete coarse aggregates. *Constr Build Mater* 2010;24:1616–20.
- [26] Casuccio M, Torrijos M, Giaccio G, Zerbinò R. Failure mechanism of recycled aggregate concrete. *Constr Build Mater* 2012;22:1500–6.
- [27] Xiao J, Li W, Sun Z, Shah S. Crack propagation in recycled aggregate concrete under uniaxial compressive loading. *ACI Mater J* 2012;109(4):451–62.
- [28] Du T, Wang W, Liu Z, Lin H, Guo T. The complete stress-strain curve of recycled aggregate concrete under uniaxial compression loading. *J Wuhan Univ Technol-Mater Sci Ed* 2010;25(5):862–5.
- [29] Li J, Xiao J, Huang J. Microplane model for recycled aggregate concrete. In: 2nd international conference on waste engineering and management - ICWEM 2010; 2010.
- [30] Simo J, Miehe C. Associative coupled thermoplasticity at finite strains: formulation, numerical analysis and implementation. *Comput Method Appl Mech* 1992;98(1):41–104.
- [31] Svedberg T, Runesson K. A thermodynamically consistent theory of gradient-regularized plasticity coupled to damage. *Int J Plast* 1997;13(6–7):669–96.
- [32] Pamin J. Gradient-dependent plasticity in numerical simulation of localization phenomena [Ph.D. thesis]. The Netherlands: TU-Delft; 1994.
- [33] Silva R, de Brito J, Dhir R. Tensile strength behavior of recycled aggregate concrete. *Constr Build Mater* 2015;83:108–18.
- [34] Li W, Xiao J, Sun Z, Kawashima S, Shah S. Interfacial transition zones in recycled aggregate concrete with different mixing approaches. *Constr Build Mater* 2012;35:1045–55.
- [35] Willam K, Etse G. Failure assessment of the extended Leon model for plain concrete. In: SCI-C conf. Zell and See, Austria. Swansea, UK: Pineridge Press; 1990. p. 851–70.
- [36] Van Mier JGM. Fracture processes of concrete. CRC Press; 1997.
- [37] Vrech S, Etse G. Discontinuous bifurcation analysis in fracture energy-based gradient plasticity for concrete. *Int J Solids Struct* 2012;49(10):1294–303.
- [38] Hadamard J. Propagation des ondes et les equations d'Hydrodynamique. New York: Chelsea; 1903.
- [39] Vrech S, Etse G. FE approach for thermodynamically consistent gradient-dependent plasticity. *Latin Am Appl Res* 2007;37:127–32.
- [40] Akita H, Koide H, Ojima M. Tensile behavior of a recycled concrete. In: Brandt AM, Ki VC, Marshall IH, editors. Proc. inter. symp. Britte matrix composites, vol. 7. Warsaw; 2003. p. 263–8.